In situ Generation of Catalytically Relevant Nanoparticles from a Molecular Pincer Iridium Precatalyst during Polyol Deoxygenation

Rachael M. Gitnes, Maggie Wang, Ying Bao, and Margaret L. Scheuermann*

Department of Chemistry; Western Washington University; 516 High Street - MS-9150; Bellingham, WA 98225

Margaret.scheuermann@wwu.edu

KEYWORDS: iridium, hydrogenation, deoxygenation, catalyst speciation, pincer, nanoparticles

ABSTRACT: Pincer complexes such as (POCOP)Ir-based species (POCOP = κ^3-C_6H_3-1,3-[OP(R)$_2$]$_2$) are widely used as precatalysts for organic transformations with many mechanistic studies of these transformations based on the assumption that the precatalysts retain their molecular nature under catalytic conditions. We demonstrate that even ($^{t\text{Bu}}$POCOP)IrCO ($^{t\text{Bu}}$POCOP = κ^3-C_6H_3-1,3-[OP(tBu)$_2$]$_2$), a precatalyst valued for its stability, can be susceptible to the formation of nanoparticles at elevated temperatures under the acidic, reducing conditions required for polyol deoxygenation and that the nanoparticles formed in situ can contribute to the observed hydrogenation activity. The iridium nanoparticles isolated from reaction mixtures by centrifugation and detected on glass and PTFE reactor liners exhibit a high degree of aggregation and resist common cleaning protocols.

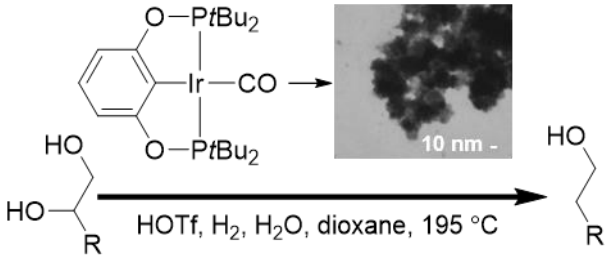

Introduction

Tridentate pincer ligands are widely used in catalytic reactions involving homogeneous transition metal catalysts.[1] Pincer ligands are valued for their strong binding and chelating abilities while their modular design allows for significant steric and electronic variation in the service of catalyst tunability.[2]

Although in situ generation of nanoparticles that are catalytically relevant, either as precatalysts or as active catalytic species, from molecular species is a known phenomenon,[3,4] reports of nanoparticle formation from pincer complexes are less common. Previous reports of metallic nanoparticle catalyst or precatalyst formation from precious metal pincer species under catalytic conditions include a rhodium-based pincer complex in an arene dehalogenation-hydrogenation system,[5] a palladium-catalyzed alkyne hydrogenation system,[6] and several palladium-based complexes employed as precatalysts in coupling reactions.[7–21] To our knowledge the formation of catalytically relevant nanoparticles from a third row metal pincer precatalyst has not been reported.

(POCOP)Ir-based pincer[22] complexes ((^{r}POCOP = κ^3-C_6H_3-1,3-[OP(R)$_2$]$_2$)) in particular have been used as precatalysts in a wide range of transformations including transfer dehydrogenation of alkanes,[23–30] heterocycles,[31] alcohols,[32] amines,[33] amine borane[34–36] and hydrazine borane,[37] the electrocatalytic reduction of CO_2,[38,39] the reduction of amides,[40,41] esters,[42] and alkyl halides,[43,44] olefin isomerization,[45,46] C–H functionalization,[47–49] the hydrosilylation of carbonyls[50,51] and CO_2,[52] silane dehydrocoupling,[53] ether C–O cleavage,[54,55] formal epoxide hydrogenation,[56] and most relevant to the present work, polyol deoxygenation.[57–59]

Polyol deoxygenation is significant in several schemes to convert biomass into value-added chemicals.[60] The ability of (POCOP)Ir species to catalyze the hydrogenation step of polyol deoxygenation reactions has been attributed to the stability of the complexes to high temperature, an acidic/aqueous environment, and harsh reducing conditions that are often required for such transformations.[57,58]

Here we demonstrate that the robust pincer ($^{t\text{Bu}}$POCOP)IrCO precatalyst ($^{t\text{Bu}}$POCOP = κ^3-C_6H_3-1,3-[OP(tBu)$_2$]$_2$) can generate nanoparticles under the reaction conditions required for polyol deoxygenation and that even the portion of the resulting nanoparticles that is deposited on the reactor liner is a sufficient precatalyst for the hydrogenation step of the polyol deoxygenation reaction. While the results presented here do not exclude the possibility of a molecular (POCOP)Ir-based catalyst in polyol deoxygenation,[61] they do suggest that the speciation of the active iridium is more complicated than previously recognized.

Results and discussion

The deoxygenation of 1,2-octanediol to 1-octanol was used as a model reaction in this study. As with previously reported polyol deoxygenation reactions involving ($^{t\text{Bu}}$POCOP)IrCO,[57,58] the deoxygenation of 1,2-octanediol to 1-octanol in the presence of acid and ($^{t\text{Bu}}$POCOP)IrCO likely proceeds by a dehydration-hydrogenation mechanism

consisting of an initial acid-catalyzed dehydration to form an aldehyde intermediate followed by and iridium-catalyzed hydrogenation. In the absence of iridium, the quantity of 1-octanol obtained is minimal indicating limited background hydrogenation activity in the reactor when a liner is in place (table 1, entry 1) confirming that the presence of iridium is essential.[62] Note that mass balance is often not obtained in dehydration-hydrogenation reactions under acidic conditions because a variety of side products can form. While none is individually is present in more than 10 % in our system, collectively they are non-trivial. Ahmed Foskey and coworkers characterized and quantified these minor species in the dehydration-hydrogenation of 1,2-propanediol.[58]

Changing the loading of (POCOP)IrCO had an insignificant impact on the yield of 1-octanol formed (table 1, entries 2 and 4) suggesting that under the conditions studied the yield of 1-octanol does not depend on the concentration of iridium. In contrast, decreasing the loading of triflic acid (table 1, entries 4 and 5) resulted in a decreased yield of 1-octanol along with a notable increase in the quantity of 1,2-octanediol starting material remaining.

Table 1. Conversion of 1,2-octane diol to 1-octanol using a ($^{t\text{Bu}}$POCOP)IrCO precatalyst

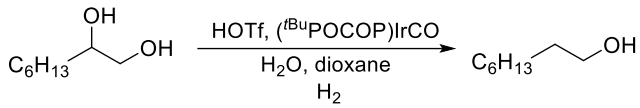

Entry[a]	Ir mol %	HOTf mol %	1-Octanol (%)[b]	1,2-Octanediol (%)
1	0	0.26	11	<1
2	0.6	0.26	70	4
3[c]	0.6	0.26	71	10
4	0.2	0.26	73	9
5	0.2	0.13	60	33

[a] Reactions were carried out in a stainless-steel reactor with a covered PTFE liner (see supporting information for a detailed description). Reaction conditions: substrate (1.2 mmol), dioxane (0.7 mL), HOTf (added as 0.17 M aq stock solution), water (180 μL), ($^{t\text{Bu}}$POCOP)IrCO (quantity varies by entry), decane (25 μL), H_2 (charged to 600 psi at 25 °C), then heated at 195 °C for 15 h. [b] Yields (relative to the initial quantity of 1,2-octane diol) measured by GC-FID using decane as an internal standard. [c] With 990 mg Hg and stirred.

After the reactions, ^{31}P NMR signals consistent with ($^{t\text{Bu}}$POCOP)IrCO and *trans*-($^{t\text{Bu}}$POCOP)IrCO(H)$_2$ were observed, indicating the same post-reaction molecular iridium speciation as was previously reported in diol deoxygenation reactions with a ($^{t\text{Bu}}$POCOP)IrCO precatalyst.[58] The purity of the ($^{t\text{Bu}}$POCOP)IrCO synthesized in our lab was confirmed by elemental analysis and after the catalytic reactions the reaction mixtures appeared clear to the naked eye.

After several reactions however a black residue was observed on the PTFE reactor liner. Examining a PTFE liner by SEM after a single reaction confirmed the presence of clusters of particles (figure 1). EDS analysis (see supporting information) confirmed the presence of iridium along with the expected fluorine signal from the PTFE (table S1). The presence of Ir was corroborated by LA-ICP-MS (figure S1). LA-ICP-MS analysis of a piece of PTFE not exposed to the reaction conditions confirmed an absence of iridium.

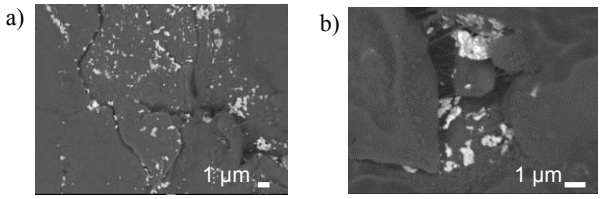

Figure 1. Backscatter electron images of a PTFE reactor liner after use in a polyol deoxygenation reaction. The bright spots indicate regions where Ir has deposited.

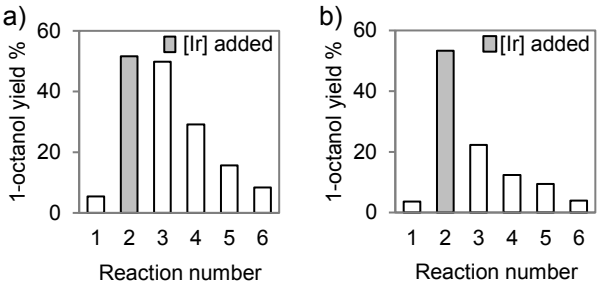

Figure 2. Catalytic performance of the ($^{t\text{Bu}}$POCOP)IrCO precatalyst and the Ir residue remaining in (a) a PTFE liner and (b) a glass liner. In both graphs reaction 1 represents a control experiment in a new liner. Reaction conditions: 1,2-octane diol (0.19 g, 1.3 mmol), dioxane (0.7 mL), HOTf (0.52 mol % added as 0.34 M aq stock solution), water (180 μL), H_2 (charged to 600 psi at 25 °C), then heated (without stirring) 195°C for 15 hours. Reaction 2 also included ($^{t\text{Bu}}$POCOP)IrCO (0.0050 g, 0.0081 mmol, 0.62 mol%). Yields measured by GC-FID using a decane (25 μL) internal standard added after the reaction.

We then investigated whether this residue could be relevant to the hydrogenation step of the diol deoxygenation reaction. An initial control experiment in the absence of iridium was performed to establish the extent of background reactivity in our reactor and liner. This established that the contribution from the steel reactor,[62] and impurities on the PTFE from polymerization or machining was minimal compared to the yields when the iridium catalyst was present (figure 2a, reaction 1). This control experiment is in addition to the one described in table 1, entry 1 and the two were not performed consecutively. This second control experiment then also confirms that if any Ir is depositing outside the covered liner on the stainless steel reactor, the catalytic contribution of this material is minimal. We then performed a reaction in the presence of the iridium catalyst. Following the reaction, the liner was cleaned with THF and acetone, two solvents in which ($^{t\text{Bu}}$POCOP)IrCO is soluble. The liner was then used for a control experiment (figure 2a, reaction 3) with all of the catalytic conditions kept constant except for the ($^{t\text{Bu}}$POCOP)IrCO which was omitted. The product yield remained

nearly identical. The rinsing procedure and control reaction steps were repeated several times and the product yields diminished on each subsequent cycle (figure 2a). We have not confirmed whether the diminished yields are explained by mechanical loss/ leaching, changes in the nature of the heterogeneous precatalyst, or both.

Because PTFE is polymeric we considered the possibility of molecular species becoming embedded in the polymer and thus resistant to removal by rinsing. Although this would not explain the observation of clusters of nanoparticles, molecular species could in theory explain the residual reactivity shown in figure 2a. To control for the possibility of molecular species embedded in the polymer we repeated the same series of experiments using glass liners. When reactions were performed in glass liners the black residue build up was also observed and the residue was imaged using SEM (figure 3). LA-ICP-MS and EDS analyses (see supporting information figure S2 and table S2 respectively) confirm that the residue is iridium-containing and that iridium-containing particles adhere to the glass surface. The residual reactivity declines more rapidly with glass compared to PTFE (figure 2b), perhaps because particles adhere less effectively to the smoother glass surface.

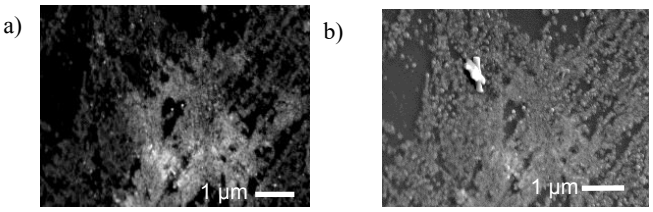

Figure 3. SEM images of a glass reactor liner after use in a polyol deoxygenation reaction. (a) Backscatter electron image, where the brighter regions indicate areas where elements of high atomic masses are present. (b) Secondary electron image showing the topography of the surface.

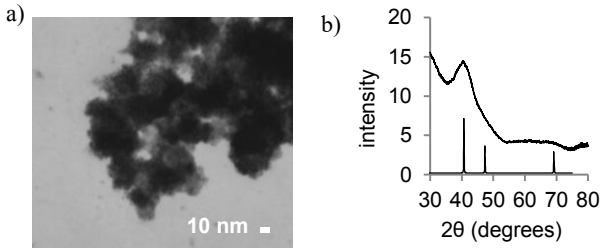

Figure 4. (a) Brightfield STEM image of aggregated nanoparticles isolated from a catalytic reaction mixture by centrifugation. (b) Powder X-Ray diffraction pattern of the aggregated nanoparticles (top) and Ir(0) (ICDD 06-0598, bottom)

Nanoparticles were isolated from the reaction mixture by centrifugation followed by washing with excess THF to remove organic impurities. The resulting solid was dispersed in ethanol, deposited on a copper grid, and characterized by STEM imaging (figure 4a) and EDS (table S3). Deposition of the isolated and purified particles onto a copper grid allowed for higher magnification than could be obtained with the carbon-coated PTFE and glass samples or with samples of the crude reaction mixture deposited onto copper grids. A sample of the centrifuged solid was also characterized by powder X-ray diffraction (figure 4b). Powder X-ray diffraction revealed a diffraction pattern consistent with metallic iridium.[63] Similar broadness has been observed in diffraction patterns of 2.5 nm Ir nanoparticles by other researchers.[64]

Efforts to quantify the extent of particle formation were hindered by the small quantity of sample involved. The quantity of nanoparticles isolated from a typical reaction mixture was less than 0.1 mg, the resolution of a laboratory balance, compared to the 5.0 mg of ($^{t\text{Bu}}$POCOP)IrCO added at the beginning of the reaction. No change in mass of the liners could be detected at the 0.1 mg level of precision. We attempted to quantify the isolated particles by analyzing suspensions of the particles by ICP-MS[65] but the results were found to be highly sensitive to variables in manipulation such as how the particles were transferred from the reactor to the centrifuge to the instrument and how quickly the samples could be drawn into the plasma after sonication.

Finke and coworkers have previously demonstrated the involvement of minimally-ligated, unsupported, non-alloyed iridium nanoparticles generated in situ from [(cod)IrCl]$_2$ (cod = cyclooctadiene) in the hydrogenation of carbon–oxygen double bonds.[66] In light of our evidence that nanoparticles may be relevant, either as precatalysts spawning smaller active clusters or as an active catalyst, we briefly investigated whether the ($^{t\text{Bu}}$POCOP)IrCO complex and its multistep synthesis were necessary. Several commercially available iridium precursors demonstrated some catalytic activity under the same conditions as the ($^{t\text{Bu}}$POCOP)IrCO precursor (table 2). The resulting residues were characterized by SEM and their catalytic performance was assessed (table S5).

Table 2. Deoxygenation of 1,2-octane diol using molecular Ir precatalysts

Entry[a]	Iridium precursor	1-Octanol (%)[b]
1	($^{t\text{Bu}}$POCOP)IrCO	71
2	[(cod)Ir(OMe)]$_2$	55
3	[Cp*IrCl$_2$]$_2$	62
4	[(cod)IrCl]$_2$	53

[a] Reactions were carried out in a stainless-steel reactor with a glass liner. Reaction conditions: substrate (0.19 g, 1.3 mmol), dioxane (0.7 mL), HOTf (0.26 mol % added as 0.17 M aq stock solution), water (180 µL), iridium source (0.0081 mmol Ir, 0.62 mol% Ir loading), decane (25 µL), H_2 (charged to 600 psi at 25 °C), then heated without stirring at 195°C for 15 hours. [b] Yields measured by GC-FID using decane as an internal standard.

The detection of nanoparticles generated from ($^{t\text{Bu}}$POCOP)IrCO under these acidic reducing conditions may have important implications for selective biomass deoxygenation, in particular, the longstanding challenge of converting glycerol to 1,3-propanediol.[67,68] A commonly invoked mechanism for this process is the dehydration-

hydrogenation mechanism[69] which has been suggested in previous deoxygenation studies involving ($^{t\text{Bu}}$POCOP)IrCO under acidic conditions.[56,57,58] Schlaf and coworkers have noted that heterogeneous catalysts for glycerol deoxygenation by dehydration-hydrogenation mechanism strongly favor the formation of 1-propanol rather than the more valuable 1,3-propanediol and suggest that this can be explained by the surface of the heterogeneous transition metal particle acting as an acid catalyst that promotes dehydration of the sterically-favored terminal position.[70] They then propose that an effective catalyst for the deoxygenation of glycerol to 1,3-propanediol by a dehydration-hydrogenation mechanism will need to be homogeneous so that the dehydration step will occur at the electronically favored internal site.

When ($^{t\text{Bu}}$POCOP)IrCO was previously investigated as a catalyst for glycerol deoxygenation it was found that the ratio of 1-propanol to 1,3-propanediol increases over time.[57] The authors of that work suggested that a change in the nature of the catalyst could be responsible. Our results along with Schlaf and coworkers' analysis suggest that the increase in 1-propanol could be the result of the formation of nanoparticles which then promote dehydration at the sterically preferred terminal carbon.

The observation of nanoparticle formation during the conversion of 1,2-octanediol to 1-octanol is also relevant to our previous report of the formal hydrogenation of terminal epoxides to primary alcohols.[56] The formal epoxide hydrogenation occurred under similar conditions to the present study and diols were observed to be rapidly formed intermediates on the pathway between the epoxides and primary alcohols.

Besides suggesting that the ($^{t\text{Bu}}$POCOP)IrCO is less stable under polyol deoxygenation conditions than was previously thought, our results also emphasize the need to perform control experiments in the middle of catalytic studies if labware is used repeatedly.[71] In addition to performing control experiments in the middle of catalytic studies, the community would benefit if the timing of these control experiments was reported as a routine detail in publications or their supporting information.

As shown in figure 2, simply rinsing with an organic solvent may not be sufficient to remove insoluble microscopic deposits of iridium nanoparticles from glass or PTFE labware. With more aggressive cleaning solutions such as base bath and aqua regia, the catalytic activity of the liners declines but the reactivity remained above the baseline level in all cases after one cleaning treatment (table 3). These observations are consistent with previous reports that complete dissolution of iridium metal is non-trivial.[72–76]

Table 3. Effect of common cleaning treatments on residual catalytic activity

Entry[a]	Cleaning treatment	1-Octanol obtained from treated PTFE liner (%)[b]	1-Octanol obtained from treated glass liner (%)[b]
1	New liner	6	3
2	THF and acetone rinses	50	22
3	Base bath soak (48 hours)	25	14
4	Aqua regia soak (48 hours)	10	16

[a] For each entry a new liner in a stainless-steel reactor was charged with substrate (0.19 g, 1.3 mmol), dioxane (0.7 mL), HOTf (0.52 mol % added as 0.34 M aq stock solution), water (180 μL), ($^{t\text{Bu}}$POCOP)IrCO (0.0081 mmol, 0.62 mol% Ir loading), H_2 (charged to 600 psi at 25 °C), then heated without stirring at 195°C for 15 hours. The liner was then subjected to the cleaning treatment at room temperature. After the cleaning treatment the liner was recharged with substrate (0.19 g, 1.3 mmol), dioxane (0.7 mL), HOTf (0.26 mol % added as 0.17 M aq stock solution), water (180 μL), H_2 (charged to 600 psi at 25 °C), then heated without stirring at 195°C for 16 hours. [b] Yields of this second reaction were measured by GC-FID using a decane (25 μL) internal standard added after the reaction.

Further our observations suggest that systematic reuse of labware could provide a quick way to identify systems where further time- and resource-intensive[3,4] investigations of potential nanoparticle involvement are appropriate.

Conclusions

The data presented here demonstrate that even pincer complexes, often regarded as robust, are not immune to the formation of nanoparticles in catalytically relevant quantities. The nanoparticles can adhere to reaction vessels made of glass and PTFE thus performing control reactions after catalytic reactions can be a useful means of screening for the potential relevance of nanoparticles in catalytic reactions. Finally, we presented data supporting the assertion that completely removing some iridium residues from labware is difficult.

AUTHOR INFORMATION

Corresponding Author

* Margaret.scheuermann@wwu.edu

Author Contributions

All authors have given approval to the final version of the manuscript.

Funding Sources

This work was supported by Western Washington University and the NSF (award # 1956353 and MRI 1532269).

ASSOCIATED CONTENT

Supporting Information. Detailed experimental procedures and data. This material is available free of charge via the Internet at http://pubs.acs.org.

ACKNOWLEDGMENT

RMG is the recipient of a Jarvis Memorial Summer Fellowship. We thank Kyle Mikkelsen for assistance with ICP-MS and Dr. Mike Kraft for assistance with SEM.

REFERENCES

[1] *Pincer and Pincer-Type Complexes: Applications in Organic Synthesis and Catalysis* [online]; Went, O. F.; Szabó, K. J., Eds.; John Wiley & Sons, Incorporated 2014; p1. ProQuest Ebook Central, http://ebookcentral.proquest.com/lib/wwu/detail.action?docID=1692003 (accessed June 23, 2020).

[2] Peris, E.; Crabtree, R. H. Key Factors in Pincer Ligand Design. *Chem. Soc. Rev.* **2018**, *47*, 1959–68.

[3] Widegren, J.; Finke, R. G. A Review of the Problem of Distinguishing True Homogeneous Catalysis from Soluble or Other Metal-Particle Heterogeneous Catalysis under Reducing Conditions. *J. Mol. Cat. A: Chem.* **2003**, 198, 317–41.

[4] Crabtree, R. H. Resolving Heterogeneity Problems and Impurity Artifacts in Operationally Homogeneous Transition Metal Catalysts. *Chem. Rev.* **2012**, *112*, 1536–1554.

[5] Buil, M. L.; Esteruelas, M. A.; Niembro, S.; Oliván, M.; Orzechowski, L.; Pelayo, C.; Vallribera, A. Dehalogenation and Hydrogenation of Aromatic Compounds Catalyzed by Nanoparticles Generated from Rhodium Bis(Imino)Pyridine Complexes. *Organometallics* **2010**, *29*, 4375–4383.

[6] Adhikary, A.; Schwartz, J. R.; Meadows, L. M.; Krause, J. A.; Guan, H. Interaction of Alkynes with Palladium POCOP-Pincer Hydride Complexes and Its Unexpected Relation to Palladium-Catalyzed Hydrogenation of Alkynes. *Inorg. Chem. Front.* **2014**, *1*, 71–82.

[7] Yu, K.; Sommer, W; Weck, M; Jones, C. W. Silica and Polymer-Tethered Pd–SCS-Pincer Complexes: Evidence for Precatalyst Decomposition to Form Soluble Catalytic Species in Mizoroki-Heck Chemistry. *J. Catal.* **2004**, *226*, 101–110.

[8] da Costa, R. C.; Jurisch, M.; Gladysz, J. A. Synthesis of Fluorous Sulfur/Carbon/Sulfur Pincer Ligands and Palladium Complexes: New Catalyst Precursors for the Heck Reaction. *Inorg. Chim. Acta* **2008**, *361*, 3205–3214.

[9] Inés, B.; SanMartin, R.; Moure, M. J.; Domínguez, E. Insights into the Role of New Palladium Pincer Complexes as Robust and Recyclable Precatalysts for Suzuki-Miyaura Couplings in Neat Water. *Adv. Synth. Catal.* **2009**, *351*, 2124–2132.

[10] Bolliger, J. L.; Frech, C. M. The 1,3-Diaminobenzene-Derived Aminophosphine Palladium Pincer Complex $\{C_6H_3[NHP(Piperidinyl)_2]_2Pd(Cl)\}$ - A Highly Active Suzuki-Miyaura Catalyst with Excellent Functional Group Tolerance. *Adv. Synth. Catal.* **2010**, *352*, 1075–1080.

[11] Bolliger, J. L.; Blacque, O.; Frech, C. M. Rationally Designed Pincer-Type Heck Catalysts Bearing Aminophosphine Substituents: Pd ^{IV} Intermediates and Palladium Nanoparticles. *Chem. Eur. J.* **2008**, *14*, 7969–7977.

[12] Bolliger, J. L.; Frech, C. M. Highly Convenient, Clean, Fast, and Reliable Sonogashira Coupling Reactions Promoted by Aminophosphine-Based Pincer Complexes of Palladium Performed under Additive- and Amine-Free Reaction Conditions. *Adv. Synth. Catal.* **2009**, *351*, 891–902.

[13] Li, J.; Lutz, M.; Spek, A. L.; van Klink, G. P. M.; van Koten, G.; Klein Gebbink, R. J. M. Novel Phosphite Palladium Complexes and Their Application in C–P Cross-Coupling Reactions. *J. Organomet. Chem.* **2010**, *695*, 2618–2628.

[14] Tamami, B.; Nezhad, M. M.; Ghasemi, S.; Farjadian, F. PCP-Pincer Palladium Nanoparticles Supported on Modified Merrifield Resin: A Novel and Efficient Heterogeneous Catalyst for Carbon–Carbon Cross-Coupling Reactions. *J. Organomet. Chem.* **2013**, *743*, 10–16.

[15] Kumar, S.; Rao, G. K.; Kumar, A.; Singh, M. P.; Singh, A. K. Palladium(Ii)-(E,N,E) Pincer Ligand (E = S/Se/Te) Complex Catalyzed Suzuki Coupling Reactions in Water via in Situ Generated Palladium Quantum Dots. *Dalton Trans.* **2013**, *42* (48), 16939.

[16] Bhaskar, R.; Sharma, A. K.; Yadav, M. K.; Singh, A. K. Sonogashira (Cu and Amine Free) and Suzuki Coupling in Air Catalyzed *via* Nanoparticles Formed *in Situ* from Pd(II) Complexes of Chalcogenated Schiff Bases of 1-Naphthaldehyde and Their Reduced Forms. *Dalton Trans.* **2017**, *46* , 15235–15248.

[17] Li, Y.; Yu, X.; Wang, Y.; Fu, H.; Zheng, X.; Chen, H.; Li, R. Unsymmetrical Pincer *N* -Heterocyclic Carbene–Nitrogen–Phosphine Chelated Palladium(II) Complexes: Synthesis, Structure, and Reactivity in Direct Csp ^{2} –H Arylation of Benzoxazoles. *Organometallics* **2018**, *37* (6), 979–988.

[18] Sharma, K. N.; Satrawala, N.; Srivastava, A. K.; Ali, M.; Joshi, R. K. Palladium(II) Ligated with a Selenated (Se, C_{NHC}, N^-)-Type Pincer Ligand: An Efficient Catalyst for Mizoroki–Heck and Suzuki–Miyaura Coupling in Water. *Org. Biomol. Chem.* **2019**, *17*, 8969–8976.

[19] Maji, A.; Singh, A.; Mohanty, A.; Maji, P. K.; Ghosh, K. Ferrocenyl Palladacycles Derived from Unsymmetrical Pincer-Type Ligands: Evidence of Pd(0) Nanoparticle Generation during the Suzuki–Miyaura Reaction and Applications in the Direct Arylation of Thiazoles and Isoxazoles. *Dalton Trans.* **2019**, *48*, 17083–17096.

[20] Gautam, P.; Tiwari, N. J.; Bhanage, B. M. Aminophosphine Palladium Pincer-Catalyzed Carbonylative Sonogashira and Suzuki–Miyaura Cross-Coupling with High Catalytic Turnovers. *ACS Omega* **2019**, *4*, 1560–1574.

[21] Maji, A.; Singh, O.; Singh, S.; Mohanty, A.; Maji, P. K.; Ghosh, K. Palladium-Based Catalysts Supported by Unsymmetrical XYC^{-1} Type Pincer Ligands: C5 Arylation of Imidazoles and Synthesis of Octinoxate Utilizing the Mizoroki-Heck Reaction: Palladium-Based Catalysts Supported by Unsymmetrical XYC^{-1} Type Pincer Ligands: C5 Arylation of Imidazoles and Synthesis of Octinoxate Utilizing the M. *Eur. J. Inorg. Chem.* **2020**, *2020*, 1596–1611.

[22] Göttker-Schnetmann, I.; White, P. S.; Brookhart, M. Synthesis and Properties of Iridium Bis(Phosphinite) Pincer Complexes (p-XPCP)IrH_2, (p-XPCP)Ir(CO), (p-XPCP)Ir(H)(Aryl), and $\{(p\text{-}XPCP)Ir\}H_2\{\mu\text{-}N_2\}$ and Their Relevance in Alkane Transfer Dehydrogenation. *Organometallics* **2004**, *23*, 1766–76.

[23] Göttker-Schnetmann, I., White, P. S.; Brookhart, M. Iridium Bis(Phosphinite) p-XPCP Pincer Complexes: Highly Active Catalysts for the Transfer Dehydrogenation of Alkanes. *J. Am. Chem. Soc.* **2004**, *126*, 1804–11.

[24] Lawrence, M. A. W.; Green, K.-A.; Nelson, P. N.; Lorraine, S. C. Review: Pincer Ligands—Tunable, Versatile and Applicable. *Polyhedron* **2018**, *143*, 11–27.

[25] Zhu, K., Achord, P. D.; Zhang, X.; Krogh-Jespersen, K.; Goldman, A. S. Highly Effective Pincer-Ligated Iridium Catalysts for Alkane Dehydrogenation. DFT Calculations of Relevant Thermodynamic, Kinetic, and Spectroscopic Properties. *J. Am. Chem. Soc.* **2004**, *126*, 13044–53.

[26] Punji, B.; Emge, T. J.; Goldman, A. S. A Highly Stable Adamantyl-Substituted Pincer-Ligated Iridium Catalyst for Alkane Dehydrogenation. *Organometallics* **2010**, *29*, 2702–9.

[27] Dinh, L. V.; Li, B.; Kumar, A.; Schinski, W.; Field, K. D.; Kuperman, A.; Celik, F. E.; Goldman, A. S. Alkyl–Aryl Coupling Catalyzed by Tandem Systems of Pincer-Ligated Iridium Complexes and Zeolites. *ACS Catal.* **2016**, *6*, 2836–41.

[28] Kumar, A.; Zhou, T.; Emge, T. J.; Mironov, O.; Saxton, R. J.; Krogh-Jespersen, K.; Goldman, A. S. Dehydrogenation of *n*-Alkanes by Solid-Phase Molecular Pincer-Iridium Catalysts. High Yields of α-Olefin Product. *J. Am. Chem. Soc.* **2015**, *137*, 9894–9911.

[29] Sheludko, B.; Cunningham, M. T.; Goldman, A. S.; Celik, F. E. Continuous-Flow Alkane Dehydrogenation by Supported Pincer-

Ligated Iridium Catalysts at Elevated Temperatures. *ACS Catal.* **2018**, *8*, 7828–41.

[30] Adams, J. J.; Arulsamy, N.; Roddick, D. M. Investigation of Iridium ^{CF3}PCP Pincer Catalytic Dehydrogenation and Decarbonylation Chemistry. *Organometallics* **2012**, *31*, 1439–47.

[31] Brayton, D. F., Jensen, C. M. Solvent Free Selective Dehydrogenation of Indolic and Carbazolic Molecules with an Iridium Pincer Catalyst. *Chem. Commun.* **2014**, *50*, 5987–89.

[32] Polukeev, A. V.; Petrovskii, P. V.; Peregudov, A. S.; Ezernitskaya, M. G.; Koridze, A. A. Dehydrogenation of Alcohols by Bis(Phosphinite) Benzene Based and Bis(Phosphine) Ruthenocene Based Iridium Pincer Complexes. *Organometallics* **2013**, *32*, 1000–1015.

[33] Bernskoetter, W. H., Brookhart, M. Kinetics and Mechanism of Iridium-Catalyzed Dehydrogenation of Primary Amines to Nitriles. *Organometallics* **2008**, *27*, 2036–45.

[34] Denney, M. C., Pons, V.; Hebden, T. J.; Heinekey, D. M.; Goldberg, K. I. Efficient Catalysis of Ammonia Borane Dehydrogenation. *J. Am. Chem. Soc.* **2006**, *128*, 12048–49.

[35] Dietrich, B. L.; Goldberg, K. I.; Heinekey, D. M.; Autrey, T.; and. Linehan, J. C. Iridium-Catalyzed Dehydrogenation of Substituted Amine Boranes: Kinetics, Thermodynamics, and Implications for Hydrogen Storage. *Inorg. Chem.* **2008**, *47*, 8583–85.

[36] Staubitz, A.; Soto, A. P.; Manners, I. Iridium-Catalyzed Dehydrocoupling of Primary Amine-Borane Adducts: A Route to High Molecular Weight Polyaminoboranes, Boron-Nitrogen Analogues of Polyolefins. *Angew. Chem. Int. Ed.* **2008**, *47*, 6212–15.

[37] Han, D.; Joksch, M.; Klahn, M.; Spannenberg, A.; Drexler, H.-J.; Baumann, W.; Jiao, H.; Knitsch, R.; Hansen, M. R.; Eckert, H.; Beweries. Iridium(III) Hydrido Complexes for the Catalytic Dehydrogenation of Hydrazine Borane. *Dalton Trans.* **2016**, *45*, 17697–704.

[38] Kang, P.; Cheng, C.; Chen, Z.; Schauer, C. K.; Meyer, T. J.; Brookhart, M. Selective Electrocatalytic Reduction of CO_2 to Formate by Water-Stable Iridium Dihydride Pincer Complexes. *J. Am. Chem. Soc.* **2012**, *134*, 5500–5503.

[39] Kang, P.; Meyer, T. J.; Brookhart, M. Selective Electrocatalytic Reduction of Carbon Dioxide to Formate by a Water-Soluble Iridium Pincer Catalyst. *Chem. Sci.* **2013**, 4, 3497–3502

[40] Park, S.; Brookhart, M. Development and Mechanistic Investigation of a Highly Efficient Iridium(V) Silyl Complex for the Reduction of Tertiary Amides to Amines. *J. Am. Chem. Soc.* **2012**, *134*, 640–53.

[41] Yuan, M.-L.; Xie, J.-H.; Zhu, S.-F.; Zhou, Q.-L. Deoxygenative Hydrogenation of Amides Catalyzed by a Well-Defined Iridium Pincer Complex. *ACS Catal.* **2016**, *6*, 3665–69.

[42] Monsigny, L.; Berthet, J.-C.; Cantat, T. Depolymerization of Waste Plastics to Monomers and Chemicals Using a Hydrosilylation Strategy Facilitated by Brookhart's Iridium(III) Catalyst. *ACS Sustain. Chem. Eng.* **2018**, *6*, 10481–88.

[43] Yang, J.; Brookhart, M. Iridium-Catalyzed Reduction of Alkyl Halides by Triethylsilane. *J. Am. Chem. Soc.* **2007**, *129*, 12656–57.

[44] Yang, J.; Brookhart, M. Reduction of Alkyl Halides by Triethylsilane Based on a Cationic Iridium Bis(Phosphinite) Pincer Catalyst: Scope, Selectivity and Mechanism. *Adv. Synth. Catal.* **2009**, *351*, 175–87.

[45] Biswas, S.; Huang, Z.; Choliy, Y.; Wang, D. Y.; Brookhart, M.; Krogh-Jespersen, K.; Goldman, A. S. Olefin Isomerization by Iridium Pincer Catalysts. Experimental Evidence for an η^3-Allyl Pathway and an Unconventional Mechanism Predicted by DFT Calculations. *J. Am. Chem. Soc.* **2012**, *134*, 13276–95.

[46] Rimoldi, M.; Fodor, D.; van Bokhoven, J. A.; Mezzetti, A. Catalytic Hydrogenation of Liquid Alkenes with a Silica-Grafted Hydride Pincer Iridium(III) Complex: Support for a Heterogeneous Mechanism. *Catal. Sci. Tech.* **2015**, *5*, 4575–86.

[47] Träff, A.; Nilsson, G. N.; Szabó, K. J.; Eriksson, L. Application of Iridium Pincer Complexes in Hydrogen Isotope Exchange Reactions. *J. Organomet. Chem.* **2007**, *692*, 5529–31.

[48] Press, L. P.; Kosanovich, A. J.; McCulloch, B. J.; Ozerov, O. V. High-Turnover Aromatic C-H Borylation Catalyzed by POCOP-Type Pincer Complexes of Iridium. *J. Am. Chem. Soc.* **2016**, *138*, 9487–9497.

[49] Hirano, M.; Fukumoto, Y.; Matsubara, N.; Chatani, N. A Cationic Iridium-Catalyzed C(sp^3)–H Silylation of 2-Alkyl-1,3-Azoles at the α-Position in the 2-Alkyl Group Leading to 2-(1-Silylalkyl)-1,3-Azoles. *Chem. Lett.* **2018**, *47*, 385–88.

[50] Park, S.; Brookhart, M. Hydrosilation of Carbonyl-Containing Substrates Catalyzed by an Electrophilic η-Silane Iridium(III) Complex. *Organometallics* **2010**, *29*, 6057–64.

[51] Park, S.; Brookhart, M. Hydrosilylation of Epoxides Catalyzed by a Cationic η^1-Silane Iridium(III) Complex. *Chem. Commun.* **2011**, *47*, 3643–45.

[52] Park, S.; Bezier, D.; Brookhart, M. An Efficient Iridium Catalyst for Reduction of Carbon Dioxide to Methane with Trialkylsilanes. *J. Am. Chem. Soc.* **2012**, *134*, 11404–7.

[53] Mucha, N. T.; Waterman, R. Iridium Pincer Catalysts for Silane Dehydrocoupling: Ligand Effects on Selectivity and Activity. *Organometallics* **2015**, *34*, 3865–72.

[54] Yang, J.; White, P. S.; Brookhart, M. Scope and Mechanism of the Iridium-Catalyzed Cleavage of Alkyl Ethers with Triethylsilane. *J. Am. Chem. Soc.* **2008**, *130*, 17509–18.

[55] Monsigny, L.; Feghali, E.; Berthet, J.-C.; Cantat, T. Efficient Reductive Depolymerization of Hardwood and Softwood Lignins with Brookhart's Iridium(III) Catalyst and Hydrosilanes. *Green Chem.* **2018**, *20*, 1981–86.

[56] Rainsberry, A. N.; Sage, J. G.; Scheuermann, M. L. Iridium-Promoted Conversion of Terminal Epoxides to Primary Alcohols under Acidic Conditions Using Hydrogen. *Catal. Sci. Technol.* **2019**, *9*, 3020–3022.

[57] Lao, D. B.; Owens, A. C. E.; Heinekey, D. M.; Goldberg, K. I. "Partial Deoxygenation of Glycerol Catalyzed by Iridium Pincer Complexes. *ACS Catal.* **2013**, *3*, 2391–96.

[58] Ahmed Foskey, T. J.; Heinekey, D. M.; Goldberg, K. I. Partial Deoxygenation of 1,2-Propanediol Catalyzed by Iridium Pincer Complexes. *ACS Catal.* **2012**, *2*, 1285–89.

[59] McLaughlin, M. P.; Adduci, L. L; Becker, J. J.; Gagné, M. R. Iridium-Catalyzed Hydrosilylative Reduction of Glucose to Hexane(s). *J. Am. Chem. Soc.* **2013**, *135*, 1225–27.

[60] Takkellapati, S.; Li, T.; Gonzalez, M. A. An Overview of Biorefinery-Derived Platform Chemicals from a Cellulose and Hemicellulose Biorefinery. *Clean Techn. Environ. Policy* **2018**, *20*, 1615–1630.

[61] Goldberg, J. M.; Goldberg, K. I.; Heinekey, D. M.; Burgess, S. A.; Lao, D. B.; Linehan, J. C. Detection of an Iridium–Dihydrogen Complex: A Proposed Intermediate in Ionic Hydrogenation. *J. Am. Chem. Soc.* **2017**, *139*, 12638–12646.

[62] Di Mondo, D.; Ashok, D.; Waldie, F.; Schrier, N.; Morrison, M.; Schlaf, M. Stainless Steel As a Catalyst for the Total Deoxygenation of Glycerol and Levulinic Acid in Aqueous Acidic Medium. *ACS Catal.* **2011**, *1*, 355–64.

[63] Swanson, H. E.; Fuyat, R. K.; Ugrinic, G. M. *Standard X-ray Diffraction Powder Patterns*; National Bureau of Standards Circular 539 Vol IV; United States Department of Commerce, National Bureau of Standards: U. S. Government Printing Office: Washington, D. C., 1955.

[64] Zhang, T.; Li, S.-C.; Zhu, W.; Ke, J.; Yu, J.-W.; Zhang, Z.-P.; Dai, L.-X.; Gu, J.; Zhang, Y.-W. Iridium Ultrasmall Nanoparticles, Wormlike Chain Nanowires, and Porous Nanodendrites: One-Pot Solvothermal Synthesis and Catalytic CO Oxidation Activity. *Surface Sci.* **2016**, *648*, 319–327.

[65] Brown, A. L.; Winter, H.; Goforth, A. M.; Sahay, G.; Sun, C. Facile Synthesis of Ligand-Free Iridium Nanoparticles and Their In Vitro Biocompatibility. *Nano. Res. Lett.* **2018**, *13*, 208–13.

[66] Özkart, S.; Finke, R. G. Iridium(0) Nanocluster, Acid-Assisted Catalysis of Neat Acetone Hydrogenation at Room Temperature:

Exceptional Activity, Catalyst Lifetime, and Selectivity at Complete Conversion. *J. Am. Chem. Soc.* **2005**, *127*, 4800–4808.

[67] Johnson, D. T.; Taconi, K. A. The Glycerin Glut: Options for the Value-Added Conversion of Crude Glycerol Resulting from Biodiesel Production. *Environ. Progress* **2007**, *26*, 338–48.

[68] ten Dam, J.; Hanefeld, U. Renewable Chemicals: Dehydroxylation of Glycerol and Polyols. *ChemSusChem* **2011**, *4*, 1017–34.

[69] Wang, Y.; Zhou, J.; Guo, X. Catalytic Hydrogenolysis of Glycerol to Propanediols: A Review. *RSC Adv.* **2015**, *5*, 74611–28.

[70] Dykeman, R. R.; Luska, K. L.; Thibault, M. E.; Jones, M. D.; Schlaf, M.; Khanfar, M.; Taylor, N. J.; Britten, J. F.; Harrington, L. Catalytic Deoxygenation of Terminal-Diols under Acidic Aqueous Conditions by the Ruthenium Complexes [(η^6-Arene)Ru(X)(N∩N)](OTf)$_n$, X = H_2O, H, η^6-arene = p-Me-^{i}Pr-C_6H_4, C_6Me_6, N∩N = bipy, phen, 6,6′-diamino-bipy, 2,9-diamino-phen, n = 1, 2): Influence of the ortho-amine substituents on catalytic activity *J. Mol. Catal. A: Chem.* **2007**, *277*, 233–51.

[71] Pentsak, E. O.; Eremin, D. B.; Gordeev, E. G.; Ananikov, V. P. Phantom Reactivity in Organic and Catalytic Reactions as a Consequence of Microscale Destruction and Contamination-Trapping Effects of Magnetic Stir Bars. *ACS Catal.* **2019**, *9*, 3070–81.

[72] Wichers, E.; Schlecht, W. G.; Gordon, C. L. Attack of Refractory Platiniferous Materials by Acid Mixtures at Elevated Temperatures. *J. Res. Natl. Bur. Stan.* **1944**, *33*, 363–81.

[73] Styrkas, A. D.; Styrkas, D. Electrochemical Dissolution of Metals of the Platinum Group by Alternating Current. *J. Appl. Electrochem.* **1995**, *25*, 490-494.

[74] Hodgson, A. P. J.; Jarvis, K. E.; Grimes, R. W.; Marsden, O. J. Development of an Iridium Dissolution Method for the Evaluation of Potential Radiological Device Materials. *J. Radioanal. Nucl. Chem.* **2016**, *307*, 2181–2186.

[75] Hodgson, A. P. J.; Jarvis, K. E.; Grimes, R. W.; Marsden, O. J. Advances in the Development of a Dissolution Method for the Attribution of Iridium Source Materials. *J. Radioanal. Nucl. Chem.* **2017**, *311*, 1193–1199.

[76] Kobayashi, Y.; Yamada, S.; Nagai, T. New Dissolution Process of Iridium to Hydrochloric Acid. In *Rare Metal Technology 2019*; Azimi, G., Kim, H., Alam, S., Ouchi, T., Neelameggham, N. R., Baba, A. A., Eds.; The Minerals, Metals & Materials Series; Springer International Publishing: Cham, 2019; pp 197–200.

TOC